

## Exact time-dependent density-functional theory for nonperturbative dynamics of the helium atom

Davood Dar <sup>1</sup>, Lionel Lacombe <sup>1</sup>, Johannes Feist <sup>2</sup> and Neepa T. Maitra <sup>1,\*</sup>

<sup>1</sup>*Department of Physics, Rutgers University, Newark 07102, New Jersey, USA*

<sup>2</sup>*Departamento de Física Teórica de la Materia Condensada and Condensed Matter Physics Center (IFIMAC), Universidad Autónoma de Madrid, Madrid, Spain*

 (Received 17 May 2021; revised 25 August 2021; accepted 26 August 2021; published 22 September 2021)

By inverting the time-dependent Kohn-Sham equation for a numerically exact dynamics of the helium atom, we show that the dynamical step and peak features of the exact correlation potential found previously in one-dimensional models persist for real three-dimensional systems. We demonstrate that the Kohn-Sham and true current densities differ by a rotational component. The results have direct implications for approximate time-dependent density functional theory calculations of atoms and molecules in strong fields, emphasizing the need to go beyond the adiabatic approximation, and highlighting caution in the quantitative use of the Kohn-Sham current.

DOI: [10.1103/PhysRevA.104.032821](https://doi.org/10.1103/PhysRevA.104.032821)

### I. INTRODUCTION

For simulating dynamics of electrons in nonperturbative fields, time-dependent density functional theory (TDDFT) [1–4] has emerged as a key approach due to its favorable system-size scaling. In theory, TDDFT is an exact formulation of quantum mechanics, which provides a computationally tractable approach for tackling calculations involving many-body problems in external time-dependent fields. Mapping to a noninteracting system, the Kohn-Sham (KS) system, that exactly reproduces the one-body density allows the computation of much larger systems than with traditional wave-function methods, with no restriction on the strength of the applied fields nor on how far the system is driven from equilibrium, see Refs. [5–10] for examples in a range of recent applications.

TDDFT does not, however, come without its own difficulties; in particular, the exchange-correlation (xc) potential in which the many-body effects are “hidden” needs to be approximated as a functional of density, and the exact xc potential depends on the density in a spatially and time nonlocal way. This dependence is neglected in adiabatic approximations used in calculations today, where the instantaneous density is inserted into a ground-state xc approximation. A crucial question is how well these approximations accurately capture the true dynamics. The lack of memory dependence is believed to be responsible for errors in its predictions, e.g., Refs. [11–22], including sometimes qualitative failures. Still, the approximations are often accurate enough to be useful, and some characterization of when to expect the adiabatic approximation to work well has also been done [23]. Studies of the exact xc potential have been made to compare against approximate potentials, and also to study the impact of its features on

the resulting dynamics. Such studies require two ingredients: first, an exact calculation of dynamics of interacting electrons and second, an inversion of the TDKS equations to find the exact potential. Because of the challenges in obtaining these ingredients, the studies have so far been limited to model systems [23–39] involving either one dimension and/or two electrons, or involving only small perturbations away from the ground state.

In this work, the exact time-dependent KS (TDKS) potential is found for a real three-dimensional (3D) multi-electron atom in the nonperturbative regime. We find dynamical step and peak features that have a nonlocal-in-space and nonlocal-in-time dependence on the density. The results have direct implications for TDDFT calculations of atoms and molecules driven far from their ground state, as these features are missing in adiabatic approximations. They justify the relevance of the previous one-dimensional (1D) studies, where similar dynamical step and peak features are found in the correlation potential. Moreover, the example explicitly demonstrates that the KS current density differs from the true current density by a rotational component. Although this has been recognized before to be theoretically possible [35,40–43], not only is this difference neglected in applications today where typically the current calculated from the KS orbitals is assumed to represent the true current [44,45], but the difference has not been demonstrated for systems beyond the linear response regime.

### II. DYNAMICS IN THE HELIUM ATOM

The system we study is the field-free evolution of a superposition state of the helium atom, as might be reached, for example, by applying a field that is turned off after some time. The lowest few eigenstates of this atom were found using the time-dependent close-coupling method, making a partial wave expansion in coupled spherical harmonics, and using the finite element discrete variable representation to

\*neepa.maitra@rutgers.edu

discretize the radial degrees of freedom [46,47]. We consider here linear superpositions of the singlet ground state,  $1^1S_0$ , denoted  $\Psi_0$ , and the singlet first excited state  $2^1P_1$  that has angular quantum numbers  $L = 1$  and  $M = 0$ , denoted here  $\Psi_1$ , so the exact time evolution of the two-electron state is

$$|\Psi(t)\rangle = \frac{1}{\sqrt{1 + |a|^2}}(|\Psi_0\rangle + ae^{-i\omega t}|\Psi_1\rangle), \quad (1)$$

where  $\omega = E_{2^1P} - E_{1^1S} = 0.77980$  in atomic units (a.u.) is the frequency with which the system oscillates. The parameter  $a$  gives the relative fraction of the excited state, for example,  $a = 1$  in the case of a 50:50 superposition. We aim then to find the time-dependent KS potential which reproduces the exact density of the interacting state Eq. (1)

$$n(\mathbf{r}, t) = \frac{1}{1 + |a|^2} [n_0(\mathbf{r}) + |a|^2 n_1(\mathbf{r}) + 2an_{01}(\mathbf{r}) \cos(\omega t)], \quad (2)$$

where  $n_q(\mathbf{r}) = 2 \int |\Psi_q(\mathbf{r}, \mathbf{r}_2)|^2 d^3\mathbf{r}_2$ ,  $q = 0, 1$  and  $n_{01}(\mathbf{r}) = 2 \int \Psi_0(\mathbf{r}, \mathbf{r}_2)\Psi_1(\mathbf{r}, \mathbf{r}_2) d^3\mathbf{r}_2$ .

We note here that the results we find for the xc potential apply to far more general dynamical situations than the field-free superposition state dynamics: due to an exact condition [48], the xc potential applies to *any* situation where the instantaneous interacting state is given by Eq. (1) at some time  $t$ , and the KS state is a Slater determinant (see Appendix A).

Now, the TDDFT xc potential depends on the choice of the initial KS state [1,37,49]; the 1-1 density-potential mapping holds only for a given initial state, which endows  $v_{xc}(\mathbf{r}, t)$  with a functional dependence on both the true and KS states,  $v_{xc}[n; \Psi(0), \Phi(0)](\mathbf{r}, t)$ . In principle, one can begin in any initial KS state that reproduces the density of the initial interacting state and its first time-derivative; the structure of the exact xc potential has a strong dependence on this choice [25,28,31,32,37]. The choice we make here is a Slater determinant: this is the natural choice if the state Eq. (1) is reached from applying an external field to a ground state and then turning the field off. The Slater determinant is the natural choice in most physical situations because these situations begin in the ground state (See also discussion in Appendix A). One would use ground-state DFT to find the initial KS orbitals, and by the ground-state theorems, this is a Slater determinant. Since the KS evolution involves a one-body Hamiltonian, the state remains a single Slater determinant. For our two-electron spin-singlet system, this means that we always have a single spatial KS orbital that is doubly occupied, and must have the form

$$\varphi(\mathbf{r}, t) = \sqrt{n(\mathbf{r}, t)/2} e^{i\alpha(\mathbf{r}, t)} \quad (3)$$

to reproduce the exact interacting density of Eq. (2) with the phase  $\alpha$  related to the current  $\mathbf{j}$  through the equation of continuity

$$\nabla \cdot \mathbf{j} = \nabla \cdot [n(\mathbf{r}, t)\nabla\alpha(\mathbf{r}, t)] = -\frac{\partial}{\partial t}n(\mathbf{r}, t). \quad (4)$$

Inverting the TDKS equation yields the exact KS potential

$$v_s(\mathbf{r}, t) = \frac{\nabla^2 \sqrt{n(\mathbf{r}, t)}}{2\sqrt{n(\mathbf{r}, t)}} - \frac{|\nabla\alpha(\mathbf{r}, t)|^2}{2} - \frac{\partial\alpha(\mathbf{r}, t)}{\partial t}. \quad (5)$$

The exact xc potential is then obtained from

$$v_{xc}(\mathbf{r}, t) = v_s(\mathbf{r}, t) - v_H(\mathbf{r}, t) - v_{ext}(\mathbf{r}, t) \quad (6)$$

with the Hartree potential  $v_H(\mathbf{r}, t) = \int \frac{n(\mathbf{r}', t)}{|\mathbf{r}-\mathbf{r}'|} d^3\mathbf{r}'$  and external potential  $v_{ext}(\mathbf{r}, t) = -2/|\mathbf{r}|$ . Further, one can isolate the correlation component by noting that for our choice of KS state,  $v_x(\mathbf{r}, t) = -v_H(\mathbf{r}, t)/2$ .

Thus, finding the exact xc potential reduces to solving Eq. (4) for  $\alpha(\mathbf{r}, t)$ . We note here that for a different choice of initial KS state, e.g., using a two-configuration state that is more similar to that of the actual interacting state, the inversion to find  $v_{xc}$  involves an iterative numerical procedure [51–53]; some examples for the 1D analog of the dynamics here can be found in Refs. [28,31,32]. This could be a more natural state to begin the KS calculation in some situations, e.g., if the state was prepared in such a superposition at the initial time, however, it is inaccessible in a KS evolution that begins in the ground state, as discussed earlier. The importance of judiciously choosing the KS initial state when using an adiabatic approximation has been realized and exploited in strong-field charge-migration simulations [9,54,55].

Equation (4) has the form of a Sturm-Liouville equation, which has a unique solution for  $\alpha(\mathbf{r}, t)$  for a given boundary condition. Thanks to the azimuthal symmetry of our density ( $M = 0$  at all times), we need solve this in effectively two dimensions. We construct an explicit matrix representation of the operator  $\nabla \cdot n(\mathbf{r}, t)\nabla$  in spherical coordinates using the fourth-order finite difference scheme subject to the following boundary conditions:

$$\alpha(\mathbf{r} \rightarrow \infty, t) = 0 \quad \text{and} \quad \frac{\partial}{\partial \theta}\alpha(\mathbf{r}, t)|_{\theta=\pi, 0} = 0. \quad (7)$$

Choosing this boundary condition at  $t = 0$  yields  $\alpha(\mathbf{r}, 0) = 0$  since initially the current is zero, and fixes our initial state as  $\phi(\mathbf{r}, 0) = \sqrt{n(\mathbf{r}, 0)}/2$ . The Runge-Gross theorem then ensures that there is a unique  $v_{xc}(\mathbf{r}, t)$  that reproduces the exact  $n(\mathbf{r}, t)$  and yields a unique  $\alpha(\mathbf{r}, t)$  at later times [56].

Subject to the boundary conditions Eq. (7), the numerical inversion of the matrix operator  $\nabla \cdot n(\mathbf{r}, t)\nabla$  results in the solution of Eq. (4) for  $\alpha(\mathbf{r}, t)$  which, in turn, when inserted into Eq. (5) yields the KS potential  $v_s(\mathbf{r}, t)$  (some details in Appendix B).

### III. RESULTS

Several symmetry features of the dynamics of our system simplify the analysis. The azimuthal symmetry mentioned earlier together with the fact that the chosen superposition is one of an  $L = 0$  and  $L = 1$  state, mean that the density, current, and potentials in the lower half-plane ( $\pi/2 < \theta < \pi$ ) exactly follow those in the upper half-plane ( $0 < \theta < \pi/2$ ) a half-cycle out of phase as  $O(r, \pi - \theta, t) = O(r, \theta, t + T/2)$ . (See also movies of the density, current-density, and correlation potentials in Supplemental Material [50]). Further the simple form of the superposition means that  $O(\mathbf{r}, T - t) = O(\mathbf{r}, t)$ . Thus we show time snapshots only over a half cycle in the lower octant.

Figure 1 shows snapshots of the correlation potential indicated by fractions of the period of oscillation  $T = 2\pi/\omega = 8.057$  a.u. One immediately notices the unmistakable

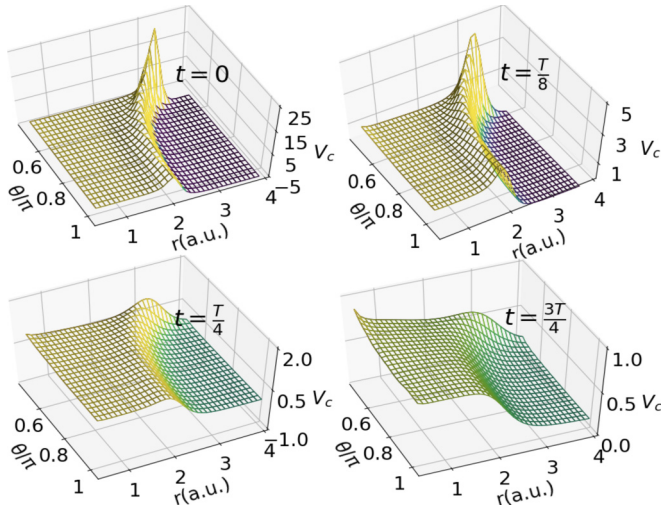


FIG. 1. Correlation potential  $v_c(\mathbf{r}, t)$  at  $t = 0$  for the 50:50 superposition case ( $\alpha = 1$ ) in the range  $\pi/2 < \theta < \pi$  at times  $t = 0, T/8, 3T/4$ , and  $T/2$ .

presence of the step and peak features in the exact correlation potential that have been shown to arise in many 1D model systems [23–34]. The step and peak feature is initially most prominent in the region swept by  $\pi/2 < \theta < \pi$ , and then decreases in magnitude, gliding out of this region and appearing on the other side of  $\theta = \pi/2$  at  $t = T/2$ . As in the 1D case, this time-dependent step has a spatially nonlocal and nonadiabatic dependence on the density and is completely unaccounted for in the adiabatic approximations: It is missing even in the exact adiabatic approximation, i.e., evaluating the exact ground-state xc potential on the instantaneous density [24–27,29]. These features often dominate the KS potential (see Fig. 2) and have been shown to be responsible for various errors in simulations using adiabatic approximations in one dimension, e.g., Refs. [25,29]. Here we find they persist just as vigorously, with the same order of magnitude, in real 3D atoms driven far from their ground state. This justifies

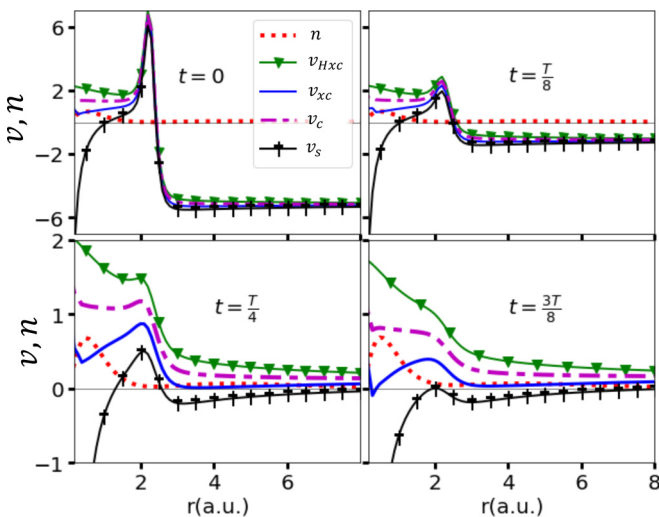


FIG. 2. Snapshots of potentials  $v_s, v_{Hxc}, v_{xc}, v_c$  and density  $2\pi r^2 n$  at  $\theta = 3\pi/4$ ,  $t = 0, T/8, T/4, 3T/8$ .

the relevance for real systems of the conclusions drawn from the 1D studies, and shows that such strong correlation effects are not a consequence of reduced dimensionality, as might have been assumed from ground-state systems [57]. These dynamical steps are distinct to those arising from fractional charges [38,58,59], or in response situations [60], as in the 1D case, and we expect they generically appear when a system is driven far from its ground state.

For the dynamics of this particular superposition state, at any instant of time, the correlation potential asymptotes to the same (time-dependent) value in every direction in the lower half plane, while asymptoting to a different value in the upper half plane [recall  $O(\mathbf{r}, T - t) = O(\mathbf{r}, t)$ ]. At  $\theta = \pi/2$  there is a step and peak in  $v_c$  in the  $\theta$  direction which gives a force that ensures KS currents, like the true currents, do not cross the  $xy$  plane. This complex structure makes the inversion numerically unreliable right at  $\theta = \pi/2$ . Along the  $\theta = \pi/2$  plane, the density of the  $P$  state vanishes, and the large change in the potential may be somewhat reminiscent of the abnormal divergent behavior along the highest-occupied molecular orbital (HOMO) nodal plane found in the ground-state potential [61]. Unlike the ground-state case, however, our density does decay differently along that plane than in other directions, and moreover cannot be captured by any adiabatic approximation.

Decomposing the terms in Eq. (5), we find that the peak tends to arise from the second term while the third term results in the step. Because the KS current  $\mathbf{j}_s = n\nabla\alpha$ , the second term and the peak are related to the local velocity  $\mathbf{j}_s/n$ , while the step when a cut is taken across a fixed  $\theta$  is related to the radial integral of the local acceleration,  $\dot{\alpha}(r, t) = \int^r \nabla \dot{\alpha}(r', t) \cdot \hat{r}' dr'$ .

We note that the appearance of such dominating steps in the correlation potential is fundamentally linked to the difference in configurations of the interacting and KS states: the interacting system is a superposition of a ground and excited state, quite distinct from the KS Slater determinant structure. Tuning down the electron-interaction dampens the peak structure, but the step remains.

Figure 2 shows the components of the exact KS potential. We observe that, in the central region where most of the density is localized, the force from the correlation potential is much smaller than that from the exchange and Hartree terms. It is, in fact, of similar magnitude to that in the ground state [62]. Near the density minimum, where the excited state begins to dominate over the ground state, the correlation potential rises, and then falls before leveling out. In this region, the slopes are such that the step appears to be keeping different parts of the density separate, while the peak corrects for dynamical Coulombic electron-interaction effects. The lack of these features in the adiabatic approximations suggests that the resulting densities will not be as structured, and will tend to underestimate oscillation amplitudes in the dipole moment (as seen in the 1D case [32]).

Taking different superpositions of the ground and excited states shows that the step and peak features are universally present in real 3D systems. Figure 3 shows the KS and correlation potentials at the initial time, when  $a$  in Eq. (1) is changed through 0, 0.5, 1, 2,  $\infty$ . We see that, for finite values of  $a$ , as the fraction of excited state is increased the step and peak decrease in magnitude but extend over a larger region

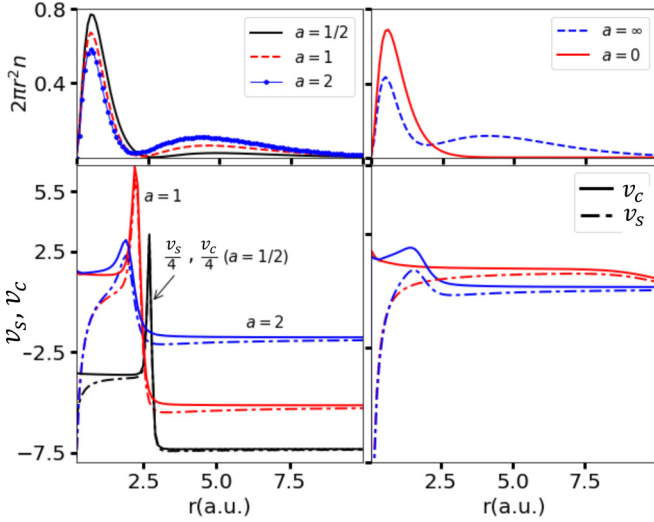


FIG. 3. Top panels: Left, initial densities for superposition states, 20:80 ( $a = 2$ ), 50:50 ( $a = 1$ ), and 80:20 ( $a = 1/2$ ). Right, ground state ( $a = 0$ ) and excited state ( $a = \infty$ ) densities. Lower panels: The corresponding KS and correlation potentials.

and move inward where more of the density is. The very sharp peak and large step seen when  $a = 0.5$  (note it is scaled to fit on the plot) occur at a sharp minimum of the density and has a smaller impact on the ensuing dynamics than the softer but still prominent structures at large  $a$  occurring in regions of greater density. When the excited state is fully occupied ( $a = \infty$ ) the KS potential is such to maintain the constant excited  $^1P$  density at all times with a noninteracting doubly occupied orbital, and the structure is not unlike that seen in the corresponding 1D excited helium atom of Ref. [37] in both magnitude and shape; again, even the adiabatically exact potential would have a completely different structure.

#### IV. TRUE AND KOHN-SHAM CURRENTS

Finally, we ask, how closely does the exact KS system reproduce the exact interacting current in this case? It was recognized in the early days of TDDFT that the exact KS current could differ from the true current by a rotational component [35,40–43], but how large this difference could be for realistic systems in the nonperturbative regime was unknown. The KS and true currents are equal in their longitudinal component, thanks to the equation of continuity,  $\nabla \cdot \mathbf{j} = -\frac{\partial n}{\partial t}$ , but they can differ in their rotational component. Indeed, for the two-electron singlet case with the KS system represented by a Slater determinant, it follows from Eq. (3) that  $\mathbf{j}_s(\mathbf{r}, t) = n(\mathbf{r}, t)\nabla\alpha(\mathbf{r}, t)$ . This implies that the true current density would need to satisfy  $\nabla \times (\mathbf{j}/n) = 0$  in order for the KS current to possibly be equal to it. For our chosen  $M = 0$  superposition, the rotational component of the current (which has only an azimuthal component) is comparable to the longitudinal component (a movie is given in the Supplemental Material [50]), and differs from the KS current. The fractional difference in the rotational component increases from about 10% to 20% as we increase the proportion of the excited state in Eq. (1) from  $a = 1$  to 2. This is shown in Fig. 4, where the fractional difference in the curl,

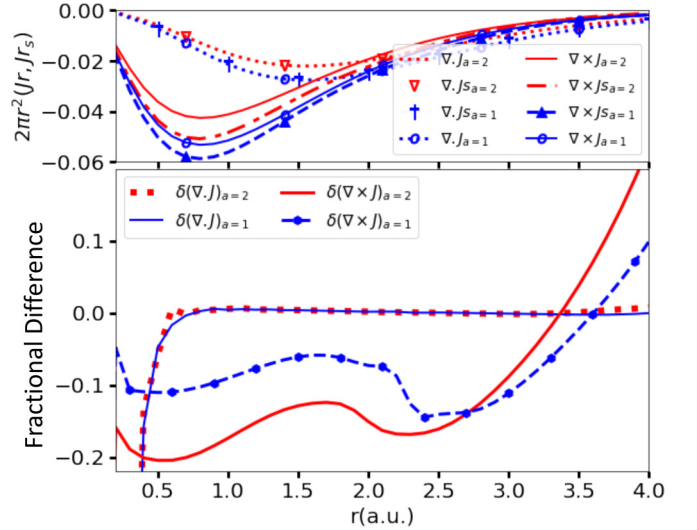


FIG. 4. Top panel: Divergence and the azimuthal component of the curl of the true and KS currents for  $a = 1$  and  $a = 2$ . Lower panel: Fractional difference  $\delta$  in the azimuthal component of curls and divergences of the current densities along  $\theta = 3\pi/4$ ,  $t = T/8$ .

$\delta(\nabla \times \mathbf{j}) = \frac{\nabla \times (\mathbf{j}_s - \mathbf{j})}{\nabla \times \mathbf{j}}$ , is contrasted with that in the divergence  $\delta(\nabla \cdot \mathbf{j}) = \frac{\nabla \cdot (\mathbf{j}_s - \mathbf{j})}{\nabla \cdot \mathbf{j}} = \frac{\nabla \cdot (\mathbf{j}_s + \partial n/\partial t)}{\nabla \cdot \mathbf{j}}$ ; the latter comes only from numerical error, and is negligible except near the origin and at large  $r$  where the denominator is very small. We note that the curl of the current is only nonzero in the azimuthal direction and this is the component of the curl that is plotted in the figure.

#### V. CONCLUSION

In summary, we showed that the nonadiabatic dynamical features of the exact correlation potential, previously seen to arise in 1D model systems, persist with comparable magnitudes in real 3D systems, and are not a consequence of reduced dimensionality. The results inform the ongoing development of more accurate functionals in TDDFT that capture these features [23,28], pressing the case to go beyond adiabatic functionals. Hybrid functionals, including range-separated ones, where nonlocal density dependence arises from the orbital dependence in an exact exchange, do not capture these features; this is particularly evident in the present two-electron case, where the exact exchange simply cancels the self-interaction in the Hartree potential. Furthermore, we demonstrated that the true interacting current differs from its KS counterpart, with the difference depending on the relative proportions of ground and excited state composing the state. The results thus advise caution when computing the current density from the KS orbitals; this will be inherently approximate even if the exact xc functional was somehow known and used.

#### ACKNOWLEDGMENTS

Financial support from the National Science Foundation Award No. CHE-1940333 (DD) and from the Department of Energy, Office of Basic Energy Sciences, Division of

Chemical Sciences, Geosciences, and Biosciences under Award No. DESC0020044 (NTM, LL) are gratefully acknowledged. J.F. acknowledges financial support from the European Research Council through Grant No. ERC-2016-StG-714870, and by the Spanish Ministry for Science, Innovation, and Universities: Agencia Estatal de Investigación through Grant No. RTI2018-099737-B-I00.

## APPENDIX A: GENERALITY OF THE RESULTS

Although the dynamics of the field-free superposition state may appear simplistic, the results obtained for the xc potential apply to far more general dynamics of the two-electron system. The results apply directly to any situation where the state is in the superposition of the ground and first-excited He atom states we considered in Eq. (1) (the singlet  $M = 0$  states  $1^1S$  and  $2^1P$ ), whether in the presence of a field or not. This can be seen from considering the following exact property of the time-dependent xc potential [48]:

$$v_{xc}[n_{t'}; \Psi_{t'}, \Phi_{t'}](\mathbf{r}t) = v_{xc}[n; \Psi_0, \Phi_0](\mathbf{r}t); \quad t \geq t' > 0, \quad (\text{A1})$$

where  $\Psi_{t'}, \Phi_{t'}$  are the interacting and KS wave functions at time  $t'$  that evolved from initial wave functions  $\Psi_0, \Phi_0$  at time 0, and  $n_{t'}$  is the density everywhere in space but considered only on the time domain from time  $t'$  to  $t$ . A consequence of this exact condition is that the xc potential at any time  $t$  can be viewed directly as a functional of the interacting state at time  $t$  and the KS state at time  $t$  (taking  $t' = t$  on the left-hand side above).

This means that if we wish to find the xc potential for a state at time  $t_1$  that happens to be instantaneously in the linear superposition

$$(|1^1S\rangle + ae^{-i\omega t_1}|2^1P\rangle)/\sqrt{1+|a|^2}, \quad (\text{A2})$$

then the xc potential we found directly applies, *no matter how the system got there, nor what it will do subsequently*.

Thus, the xc potentials we found cover a large range of dynamics of the He atom and indicate a *general* feature of the xc potential in nonperturbative He dynamics. There is a limitation in that the configuration of the interacting wave function must be a linear combination of the  $1^1S$  and  $2^1P$  states at the time of interest, and that the KS wave function is chosen to be a Slater determinant (which, if chosen at the initial time as such, will always remain such), but this already covers a wide range of situations.

As a specific example, consider beginning the physical system at time 0 in the ground state and driving it to a superposition state at time  $t'$  under some external field. It follows from Eq. (A1) that at time  $t = t'$  the exact xc potential may be viewed as either a functional of the history of the

density, or, equally, as a functional purely of the states at time  $t = t'$ . Assuming we can reach the superposition state described by Eq. (A2) at any time  $t$  starting in a ground state (e.g., by a weak Rabi oscillation), then the xc potential at time  $t$  is precisely the one we found in our paper. As an explicit demonstration of this, it may be useful to note the similarities of the xc potential found for the 1D superposition state and that for the Rabi dynamics studied in Ref. [24].

## APPENDIX B: NUMERICAL DETAILS

To solve the equation

$$\nabla \cdot [n(\mathbf{r}, t)\nabla\alpha(\mathbf{r}, t)] = -\frac{\partial}{\partial t}n(\mathbf{r}, t), \quad (\text{B1})$$

we construct the explicit matrix representation of the operator  $\nabla \cdot [n(\mathbf{r}, t)\nabla\alpha(\mathbf{r}, t)]$  subject to the boundary conditions

$$\alpha(\mathbf{r} \rightarrow \infty, t) = 0 \quad \text{and} \quad \frac{\partial}{\partial\theta}\alpha(\mathbf{r}, t)|_{\theta=\pi, 0} = 0. \quad (\text{B2})$$

In the rectangular computational domain that we use to solve the problem, the grid  $(r, \theta)$  extends from  $0 \rightarrow R = 30$  a.u. in  $r$  (the density is negligible this far from the nucleus) and  $0 \rightarrow \pi$  in  $\theta$ . Consequently the boundary conditions, Eq. (B2) translate to

$$\begin{aligned} \alpha(r = R, \theta, \varphi, t) = 0, \quad \frac{\partial}{\partial\theta}\alpha(r, \theta, \varphi, t)|_{\theta=\pi} = 0, \\ \frac{\partial}{\partial\theta}\alpha(r, \theta, \varphi, t)|_{\theta=0} = 0. \end{aligned} \quad (\text{B3})$$

The finite difference approximation of the derivative operator has the nice property that the resulting matrix is sparse, and consequently the operator, which by definition is local in space, remains so in this representation as well since only a few adjacent grid points are coupled. The high sparsity of the matrix also allows for efficient computation of matrix inversion. Despite the computational efficiency it offers, caution is required to avoid numerical inaccuracies especially where the density becomes small. We ensure that our conclusions are robust with numerics, interpreting the results in regions where the inversion is accurate, and checking that the action of the matrix representing  $\nabla \cdot n(\mathbf{r}, t)\nabla$  on the solution vector  $\alpha(\mathbf{r}, t)$  agrees with the right-hand side of Eq. (B1). In a similar way, we calculate the exact Hartree potential  $v_H(\mathbf{r}, t)$ , by numerically inverting

$$\nabla^2 v_H(\mathbf{r}, t) = -4\pi n(\mathbf{r}, t), \quad (\text{B4})$$

and then use  $v_{xc}(\mathbf{r}, t) = v_s(\mathbf{r}, t) - v_H(\mathbf{r}, t) - v_{\text{ext}}(\mathbf{r}, t)$  to obtain the xc potential, and we isolate the correlation potential noting that, for our choice of KS state,  $v_x(\mathbf{r}, t) = -v_H(\mathbf{r}, t)/2$ .

- [1] E. Runge and E. K. U. Gross, *Phys. Rev. Lett.* **52**, 997 (1984).  
 [2] N. T. Maitra, *J. Chem. Phys.* **144**, 220901 (2016).  
 [3] *Fundamentals of Time-Dependent Density Functional Theory*, Vol. 837, edited by M. A. Marques, N. T. Maitra, F. M.

- Nogueira, E. K. Gross, and A. Rubio (Springer, New York, 2012).  
 [4] C. A. Ullrich, *Time-Dependent Density-Functional Theory: Concepts and Applications* (Oxford University Press, New York, 2011).

- [5] E. W. Draeger, X. Andrade, J. A. Gunnels, A. Bhatele, A. Schleife, and A. A. Correa, *J. Parallel Distributed Computing* **106**, 205 (2017).
- [6] S. A. Sato, *Comput. Mater. Sci.* **194**, 110274 (2021).
- [7] A. Guandalini, C. Cocchi, S. Pittalis, A. Ruini, and C. A. Rozzi, *Phys. Chem. Chem. Phys.* **23**, 10059 (2021).
- [8] N. Singh, P. Elliott, J. K. Dewhurst, and S. Sharma, *Phys. Rev. B* **103**, 134402 (2021).
- [9] A. S. Folorunso, A. Bruner, F. Mauger, K. A. Hamer, S. Hernandez, R. R. Jones, L. F. DiMauro, M. B. Gaarde, K. J. Schafer, and K. Lopata, *Phys. Rev. Lett.* **126**, 133002 (2021).
- [10] D. C. Yost, Y. Yao, and Y. Kanai, *Phys. Rev. B* **96**, 115134 (2017).
- [11] S. Raghunathan and M. Nest, *J. Chem. Theory Comput.* **7**, 2492 (2011).
- [12] R. Ramakrishnan and M. Nest, *Phys. Rev. A* **85**, 054501 (2012).
- [13] B. F. Habenicht, N. P. Tani, M. R. Provorse, and C. M. Isborn, *J. Chem. Phys.* **141**, 184112 (2014).
- [14] H. O. Wijewardane and C. A. Ullrich, *Phys. Rev. Lett.* **100**, 056404 (2008).
- [15] C.-Z. Gao, P. M. Dinh, P.-G. Reinhard, and E. Suraud, *Phys. Chem. Chem. Phys.* **19**, 19784 (2017).
- [16] E. V. Boström, A. Mikkelsen, C. Verdozzi, E. Peretto, and G. Stefanucci, *Nano Lett.* **18**, 785 (2018).
- [17] J. Krumland, A. M. Valencia, S. Pittalis, C. A. Rozzi, and C. Cocchi, *J. Chem. Phys.* **153**, 054106 (2020).
- [18] E. E. Quashie, B. C. Saha, X. Andrade, and A. A. Correa, *Phys. Rev. A* **95**, 042517 (2017).
- [19] C.-Z. Gao, J. Wang, F. Wang, and F.-S. Zhang, *J. Chem. Phys.* **140**, 054308 (2014).
- [20] N. Henkel, M. Keim, H. J. Lüdde, and T. Kirchner, *Phys. Rev. A* **80**, 032704 (2009).
- [21] B. Da, J. Liu, M. Yamamoto, Y. Ueda, K. Watanabe, N. T. Cuong, S. Li, K. Tsukagoshi, H. Yoshikawa, H. Iwai, S. Tanuma, H. Guo, Z. Gao, X. Sun, and Z. Ding, *Nat. Commun.* **8**, 15629 (2017).
- [22] X. Yao, Y. Lee, D. Ceresoli, and K. Cho, *J. Phys. Chem. A* **125**, 4524 (2021).
- [23] L. Lacombe and N. T. Maitra, *Faraday Discuss.* **224**, 382 (2020).
- [24] K. Luo, J. I. Fuks, E. D. Sandoval, P. Elliott, and N. T. Maitra, *J. Chem. Phys.* **140**, 18A515 (2014).
- [25] Y. Suzuki, L. Lacombe, K. Watanabe, and N. T. Maitra, *Phys. Rev. Lett.* **119**, 263401 (2017).
- [26] P. Elliott, J. I. Fuks, A. Rubio, and N. T. Maitra, *Phys. Rev. Lett.* **109**, 266404 (2012).
- [27] J. I. Fuks, P. Elliott, A. Rubio, and N. T. Maitra, *J. Phys. Chem. Lett.* **4**, 735 (2013).
- [28] L. Lacombe and N. T. Maitra, *J. Chem. Theory Comput.* **15**, 1672 (2019).
- [29] L. Lacombe, Y. Suzuki, K. Watanabe, and N. T. Maitra, *Eur. Phys. J. B* **91**, 96 (2018).
- [30] J. D. Ramsden and R. W. Godby, *Phys. Rev. Lett.* **109**, 036402 (2012).
- [31] J. I. Fuks, S. Nielsen, M. Ruggenthaler, and N. T. Maitra, *Phys. Chem. Chem. Phys.* **18**, 20976 (2016).
- [32] J. I. Fuks, L. Lacombe, S. E. B. Nielsen, and N. T. Maitra, *Phys. Chem. Chem. Phys.* **20**, 26145 (2018).
- [33] M. J. P. Hodgson, J. D. Ramsden, and R. W. Godby, *Phys. Rev. B* **93**, 155146 (2016).
- [34] M. J. P. Hodgson, J. D. Ramsden, J. B. J. Chapman, P. Lillystone, and R. W. Godby, *Phys. Rev. B* **88**, 241102(R) (2013).
- [35] R. D'Agosta and G. Vignale, *Phys. Rev. B* **71**, 245103 (2005).
- [36] M. Ruggenthaler, S. E. B. Nielsen, and R. van Leeuwen, *Phys. Rev. A* **88**, 022512 (2013).
- [37] P. Elliott and N. T. Maitra, *Phys. Rev. A* **85**, 052510 (2012).
- [38] M. Thiele, E. K. U. Gross, and S. Kümmel, *Phys. Rev. Lett.* **100**, 153004 (2008).
- [39] C. A. Ullrich, *J. Chem. Phys.* **125**, 234108 (2006).
- [40] N. T. Maitra, K. Burke, H. Appel, and E. Gross, *Rev. Mod. Quantum Chem.* **2**, 1186 (2002).
- [41] P. Schaffhauser and S. Kümmel, *Phys. Rev. B* **93**, 035115 (2016).
- [42] M. Thiele and S. Kümmel, *Phys. Rev. A* **79**, 052503 (2009).
- [43] E. Gross and N. Maitra, in *Fundamentals of Time-Dependent Density Functional Theory*, edited by M. A. Marques, N. T. Maitra, F. M. Nogueira, E. Gross, and A. Rubio (Springer, Berlin, 2012), pp. 53–99.
- [44] X. Andrade, S. Hamel, and A. Correa, *Eur. Phys. J. B* **91**, 229 (2018).
- [45] T. Takeuchi, M. Noda, and K. Yabana, *ACS Photonics* **6**, 2517 (2019).
- [46] J. Feist, Two-photon double ionization of helium, PhD Thesis, 2009.
- [47] J. Feist, S. Nagele, R. Pazourek, E. Persson, B. I. Schneider, L. A. Collins, and J. Burgdörfer, *Phys. Rev. A* **77**, 043420 (2008).
- [48] N. T. Maitra, K. Burke, and C. Woodward, *Phys. Rev. Lett.* **89**, 023002 (2002).
- [49] R. van Leeuwen, *Phys. Rev. Lett.* **82**, 3863 (1999).
- [50] See Supplemental Material at <http://link.aps.org/supplemental/10.1103/PhysRevA.104.032821> for [brief description].
- [51] M. Ruggenthaler and van Leeuwen R., *Europhys. Lett.* **95**, 13001 (2011).
- [52] S. E. B. Nielsen, M. Ruggenthaler, and R. van Leeuwen, *Europhys. Lett.* **101**, 33001 (2013).
- [53] M. Ruggenthaler, M. Penz, and R. van Leeuwen, *J. Phys.: Condens. Matter* **27**, 203202 (2015).
- [54] A. Bruner, S. Hernandez, F. Mauger, P. M. Abanador, D. J. LaMaster, M. B. Gaarde, K. J. Schafer, and K. Lopata, *J. Phys. Chem. Lett.* **8**, 3991 (2017).
- [55] M. Chen and K. Lopata, *J. Chem. Theory Comput.* **16**, 4470 (2020).
- [56] It is not *a priori* obvious that the unique solution to Eq. (4) with the boundary-condition Eq. (7) applied with time  $t$  as a parameter is compatible with the TDKS evolution, but as the results evolve smoothly in time, it is.
- [57] L. Brus, *Acc. Chem. Res.* **47**, 2951 (2014).
- [58] E. Kraiser, M. J. P. Hodgson, and E. K. U. Gross, *J. Chem. Theory Comput.* **17**, 1390 (2021).
- [59] N. T. Maitra, *J. Phys.: Condens. Matter* **29**, 423001 (2017).
- [60] S. J. A. van Gisbergen, P. R. T. Schipper, O. V. Gritsenko, E. J. Baerends, J. G. Snijders, B. Champagne, and B. Kirtman, *Phys. Rev. Lett.* **83**, 694 (1999).
- [61] P. Gori-Giorgi, T. Gál, and E. J. Baerends, *Mol. Phys.* **114**, 1086 (2016).
- [62] C. J. Umrigar and X. Gonze, *Phys. Rev. A* **50**, 3827 (1994).